Raman, Visible and Ultra-violet Spectral Studies of Ionic Interactions in Molten Alkali Nitrate and Nitrite Systems

Kazuo Sakai * and Tetsurō Nakamura

Research Laboratory of Engineering Materials, Tokyo Institute of Technology, 4259 Nagatsuta, Midoriku, Yokohama 227, Japan

Z. Naturforsch. **40 a**, 892–902 (1985); received March 9, 1985

The interaction between the various ions in the molten systems $NaNO_3$–$NaNO_2$, $LiNO_3$–$NaNO_2$ and $NaNO_3$–KNO_2 has been investigated by Raman, visible and ultraviolet absorption spectroscopy. It is concluded that the interaction between the anions is very weak and that the cations Na^+ and K^+ are randomly distributed around the nitrate and nitrite anions. The empty orbital level of Na^+ (434 nm) in $NaNO_3$–$NaNO_2$ relative to the π level of NO_2^- is estimated. When small amounts of Li^+ are added to the binary sodium melt, an anomalous spectroscopic result is obtained.

The structure and other physical properties of molten nitrate and nitrite systems have already been studied extensively by means of calorimetry [1–5], gravimetry [6], X-ray diffraction [7, 8], Raman spectroscopy [9–21], and visible and ultraviolet absorption spectroscopy [22, 23]. An investigation of the interaction between the anions in a molten system containing nitrate and iodate has also been reported [24].

However, few molten nitrate-nitrite systems, additive [25] or reciprocal [26], have been investigated. Therefore we have studied the ionic interaction in the molten systems $NaNO_3$–$NaNO_2$, $LiNO_3$–$NaNO_2$ and $NaNO_3$–KNO_2 by means of Raman, visible and ultraviolet absorption spectroscopy.

Experimental

The nitrates ANO_2 (A = Li, Na, K; 99.9%) were dehydrated in vacuo at about 40 °C for several days. Then we examined the ANO_3 purity and the absence of nitrate (820 cm^{-1} for NO_2^-) by Raman spectroscopy. In the same manner the nitrites BNO_2 (B = Na, K) were dehydrated after recrystallization. A single crystal of $NaNO_2$ was grown via the Stock-Barger method. But we failed to obtain single crystals of $LiNO_2$ and KNO_2. Therefore, we repeated the recrystallization and dehydration several times, put the samples into an alumina crucible and kept them under argon just above the melting point for 2 hrs. Again the nitrite purity was examined by Raman spectroscopy.

The purified nitrates and nitrites were mixed in the desired ratios in a dry box. Then the sample were transferred into the furnance in argon atmosphere and the temperature was raised just above the melting temperature. A part of the fused sample was transferred into the quartz Raman cell. After the temperature was decreased, the Raman cell was sealed off in vacuo.

The Raman spectra were recorded at 360 °C by a JEOL spectrometer with 514.5 nm excitation (ca. 300 mW) of an Ar ion Laser (Spectra Physics). To analyze in detail we recorded over three ranges: 650–850 cm^{-1}, 1000–1100 cm^{-1} and 1100–1600 cm^{-1}. For the 1000–1100 cm^{-1} range the spectral slit width was fixed at 1.5 cm^{-1}, for the other ranges, at 3 cm^{-1}. Each range was scanned for 50 min. The calibration was carried out by using Neon lines.

Visible (VIS) and ultraviolet (UV) absorption spectra were recorded with a single beam JASCO-SS 50 spectrophotometer using quartz sample cells placed in an electric furnace. Samples of nitrate and nitrite in the appropriate molar ratio were mixed

* Present address: Electronics Materials Laboratory, Sumitomo Metal Mining Co., Ltd., Suehirocho, Ohme, Tokyo 198, Japan.

Reprint requests to Prof. T. Nakamura, Research Laboratory of Engineering Materials, Tokyo Institute of Technology, 4259 Nagatsuta, Midoriku, Yokohama 227, Japan.

0340-4811 / 85 / 0900-0902 $ 01.30/0. – Please order a reprint rather than making your own copy.

and ground to fine powder in an Argon atmosphere, transferred into the quartz sample cell and sealed off in vacuo. Then the quartz cell was placed in the furnace. After recording reference spectra (back ground spectra of the empty part of the quartz cell) the nitrate-nitrite mixtures were equilibrated and the VIS and UV spectra measured. A Tungsten lamp was used as light source for the VIS and a Xenon lamp for the UV absorption measurements. The UV spectrometer arrangement was always purged with dried N_2.

Results

Figures 1 a–c show the Raman spectra of the $LiNO_3$–$NaNO_2$ melts. The composition changes of the A_1' mode of NO_3^- in the range of 1000–1100 cm^{-1} are shown in Figure 1 a. In a similar way, both the $E'(\nu_3)$ mode of NO_3^- and the A mode of NO_2^- in the range of 650–850 cm^{-1} are shown in Fig. 1 b and, moreover, the E' mode (ν_4) of NO_3^- and the A and B modes of NO_2^- in the range of 1100–1600 cm^{-1} are shown in Figure 1 c. Figures 2 a–c show Raman shifts vs. composition of $LiNO_3$–$NaNO_2$,

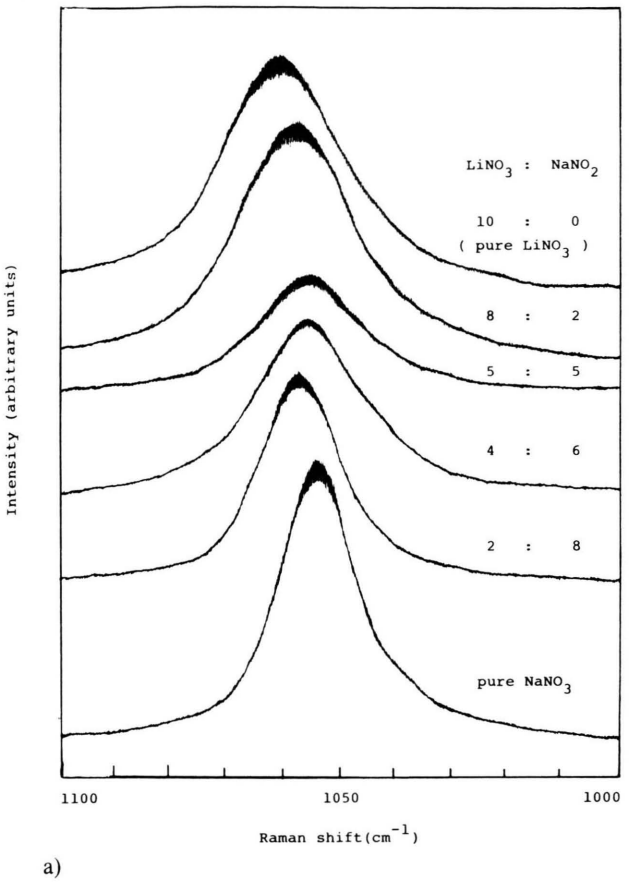

a)

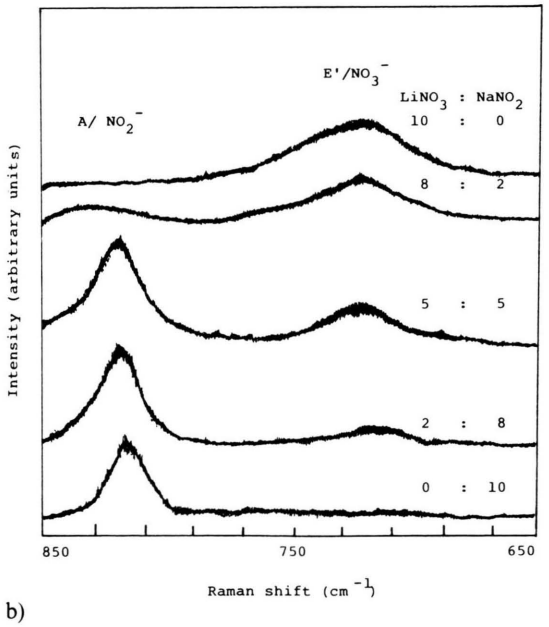

b)

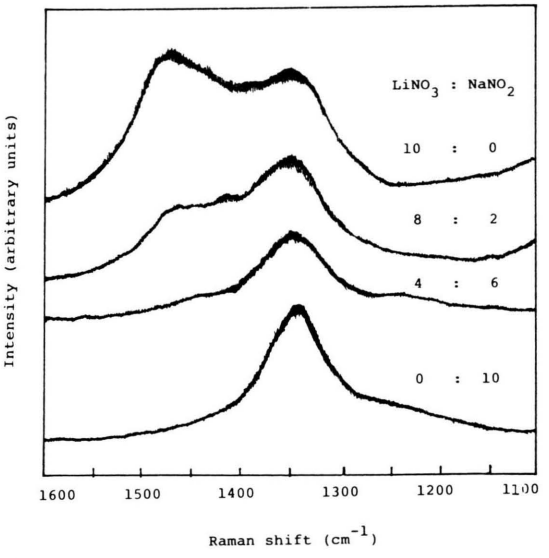

c)

Fig. 1. Raman spectra for various $LiNO_3 : NaNO_2$ ratios. a) A_1' mode of NO_3^-; b) E' mode of NO_3^- and A mode of NO_2^-; c) overlapping spectra of E' mode of NO_3^- and A and B modes of NO_2^-.

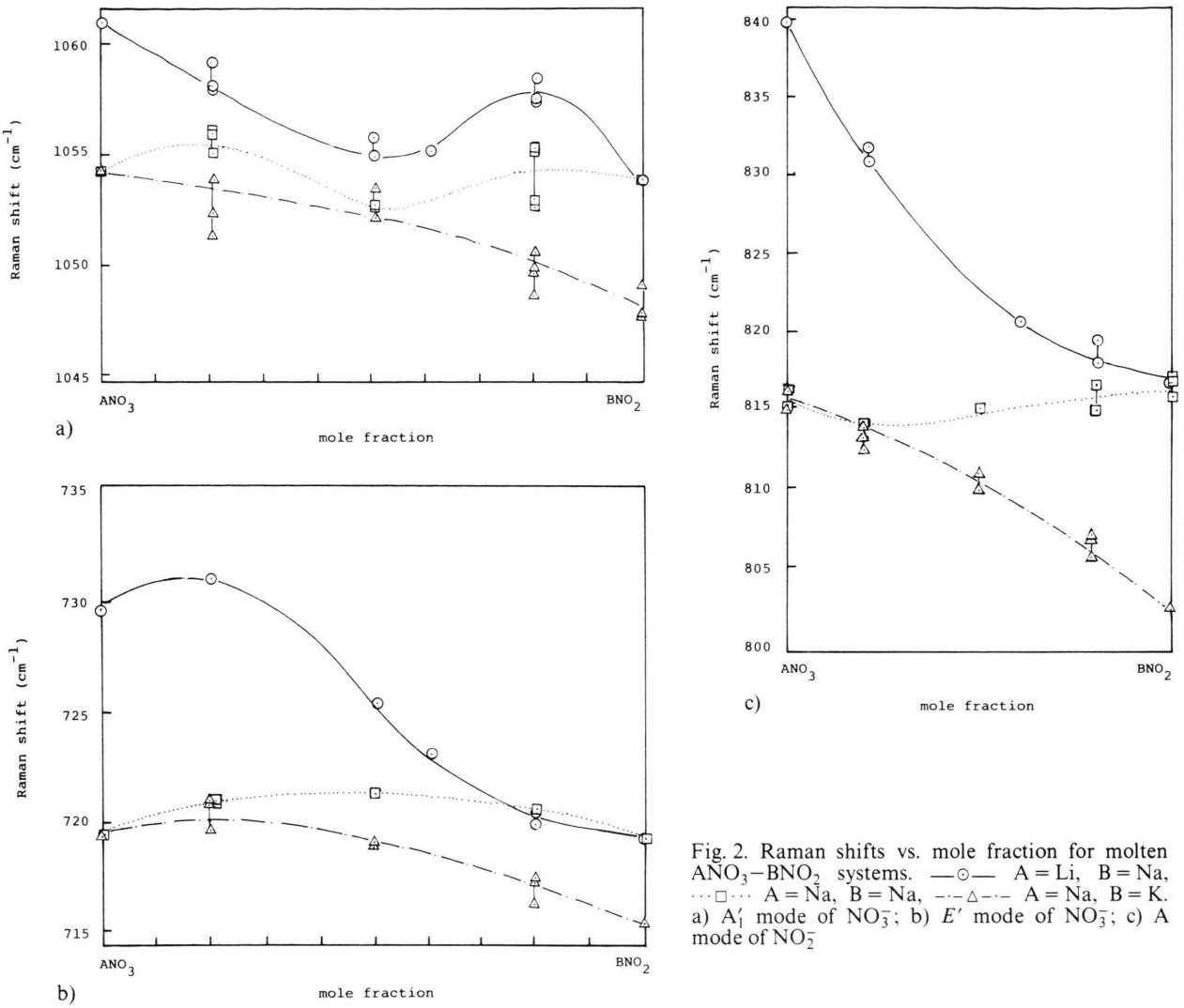

Fig. 2. Raman shifts vs. mole fraction for molten ANO_3–BNO_2 systems. —⊙— A = Li, B = Na, ···□··· A = Na, B = Na, –·–△–·– A = Na, B = K. a) A_1' mode of NO_3^-; b) E' mode of NO_3^-; c) A mode of NO_2^-

$NaNO_3$–$NaNO_2$ and $NaNO_3$–KNO_2 melts. The half widths of the A_1' mode of NO_3^- are shown in Figure 3. Figures 4a–c are examples of the deconvolution of bands by use of the non-linear least squares method with Voigt function [27], which is given by

$$V(\tilde{\nu}) = \int_{-\infty}^{+\infty} \frac{\beta_l/\pi}{\beta_l^2 + (\tilde{\nu} - \nu')^2} \frac{1}{\sqrt{\pi}\,\beta_g} \exp(-\nu'/\beta_g)\, d\nu'. \quad (1)$$

Here, β_l and β_g are half widths of Lorentzian and Gaussian functions, respectively. The relative peak intensity I, the peak center $\tilde{\nu}(\mathrm{cm}^{-1})$ and the half width $\beta_l(\mathrm{cm}^{-1})$ for individual Raman bands, separated into each Raman active mode by means of the above method, are tabulated in Table 1. The calculated force constants of NO_3^- using a Urey-Bradley potential are shown in Table 2.

The changes of the VIS absorption with composition of molten $NaNO_3$–$NaNO_2$ at 360 °C are shown in Figure 5. Figures 6a–b show VIS and UV absorption spectra, respectively, at various temperatures for the molar ratio $NaNO_3$:$NaNO_2$ = 5:5.

The absorption at 240 nm in Fig. 6b is due to the transiton from the π-orbital of NO_3^- to the empty orbital of Na^+. This absorption clearly indicates "red shift" with temperature increase. Rhodes and

Table 1. Raman shifts $\tilde{\nu}$, relative intensities I, and half widths β_1 of Raman active modes of NO_3^- and NO_2^- for various ANO_3:BNO_2 ratios [(A, B) = (Li, Na), (Na, Na), (Na, K)]. Capitals Q and P in the second column denote: Obtained by use of a quartz sample cell and a platinum basket cell, respectively. The symbol # denotes "impossible to compare"; the symbols – and * denote "no modes expected" and "failed to observe".

		$NO_3^-(A_1')$			$NO_2^-(E')$			$NO_2^-(A)$			$NO_3^-(E')+NO_2^-(A)$			$NO_2^-(B)$		
		I	$\tilde{\nu}$	β_1	I	$\tilde{\nu}$	β_1	I	$\tilde{\nu}$	β_1	I	$\tilde{\nu}$	β_1	I	$\tilde{\nu}$	β_1
$LiNO_3$:$NaNO_2$																
10 : 0	Q	#	1060.8	11.6	1.22	718.3	12.7		–		0.72	1357.5	64.2		–	
					1.00	740.9	17.0				1.00	1469.4	68.3			
8 : 2	Q	#	1059.2	11.1	1.73	720.1	12.1	0.20	813.8	7.4	1.51	1357.8	65.8		–	
					1.00	742.3	14.8				1.00	1463.9	67.1			
	P	#	1058.1	11.1		*			*			*			*	
	P	#	1057.9	11.8		*			*			*			*	
5 : 5	Q	#	1055.1	9.7		*			*			*			*	
	P	#	1055.8	9.7		*			*			*			*	
4 : 6	Q	#	1055.3	9.6	1.00	723.0	14.7	3.36	820.8	12.3	7.30	1351.3	57.9	0.78	1231.6	49.2
											1.00	1448.7	54.3			
2 : 8	Q	#	1057.4	7.5	1.00	719.8	6.3	10.04	819.6	7.6	3.93	1348.0	42.1	1.00	1261.0	81.2
	P	#	1058.6	8.1	1.00	720.1	8.4	10.58	818.1	7.9		*			*	
0 : 10	Q	#	–			–		#	816.8	8.0	8.47	1324.9	33.7	1.00	1232.0	44.5
$NaNO_3$:$NaNO_2$																
10 : 0	Q	#	1054.0	7.9	#	719.6	13.3		–		0.59	1340.2	52.8		–	
8 : 2	Q	#	1055.2	7.9	1.00	721.0	13.7	0.89	813.8	7.2	1.60	1344.9	57.2		–	
											1.00	1437.9	69.3			
	P	#	1056.0	6.7		*			*			*			*	
	P	#	1056.2	7.0		*			*			*			*	
5 : 5	Q	#	1052.5	8.1	1.00	721.3	12.1	2.32	815.0	6.5	2.28	1342.6	47.7	0.54	1250.6	78.3
											1.00	1425.7	65.7			
	P	#	1052.9	8.1		*			*			*			*	
2 : 8	Q	#	1055.3	7.5	1.00	720.6	9.7	11.57	816.6	6.5	2.13	1343.7	44.1	1.00	1232.1	78.5
	P	#	1055.8	6.9		*			*			*			*	
	Q	#	1053.0	8.7		–		#	814.9	7.4	4.36	1342.7	52.8	1.00	1232.1	78.5
	P	#	1053.4	9.1		*			*			*			*	
0 : 10	Q		–			–		#	816.6	8.0	4.27	1335.0	37.4	1.00	1231.0	49.4
$NaNO_3$:KNO_2																
10 : 0	Q	#	1054.0	7.9	#	719.6	13.3		–		0.59	1340.2	52.8		–	
											1.00	1430.7	73.4			
8 : 2	Q	#	1053.9	7.1	1.00	721.0	13.7	0.89	813.8	7.3	1.54	1341.5	51.5		–	
											1.00	1428.2	66.1			
	P	#	1051.4	7.2	1.00	719.8	13.9	0.82	814.3	7.9		*			*	
	P	#	1052.3	7.8	1.00	720.6	13.8	0.81	812.9	9.2		*			*	
5 : 5	Q	#	1052.1	6.7	1.00	718.9	10.8	3.17	810.0	6.3	2.99	1335.0	42.2	0.60	1246.7	64.1
											1.00	1407.6	75.1			
	P	#	1050.7	6.0	1.00	716.1	8.9	12.19	805.8	5.0	4.30	1331.3	38.5	1.00	1251.3	67.2
											1.00	1409.1	60.6			
2 : 8	Q	#	1050.7	6.0	1.00	716.1	8.9	12.19	805.8	5.0	4.30	1331.3	38.5	1.00	1251.3	77.1
	P	#	1050.0	6.1	1.00	717.0	9.1	9.34	806.6	6.7		*			*	
	P	#	1049.9	6.9	1.00	717.5	11.8	10.97	807.0	6.1		*			*	
0 : 10	Q		–			–		#	803.2	4.4	6.66	1340.5	33.7	1.00	1232.4	44.5
	P		–			–		#	802.2	4.7	8.00	1324.9	31.0	1.00	1231.8	40.4
KNO_3	Q	#	1048.1	5.9	#	714.7	9.4		–		1.00	1346.2	28.4		–	
											1.82	1413.4	42.9			

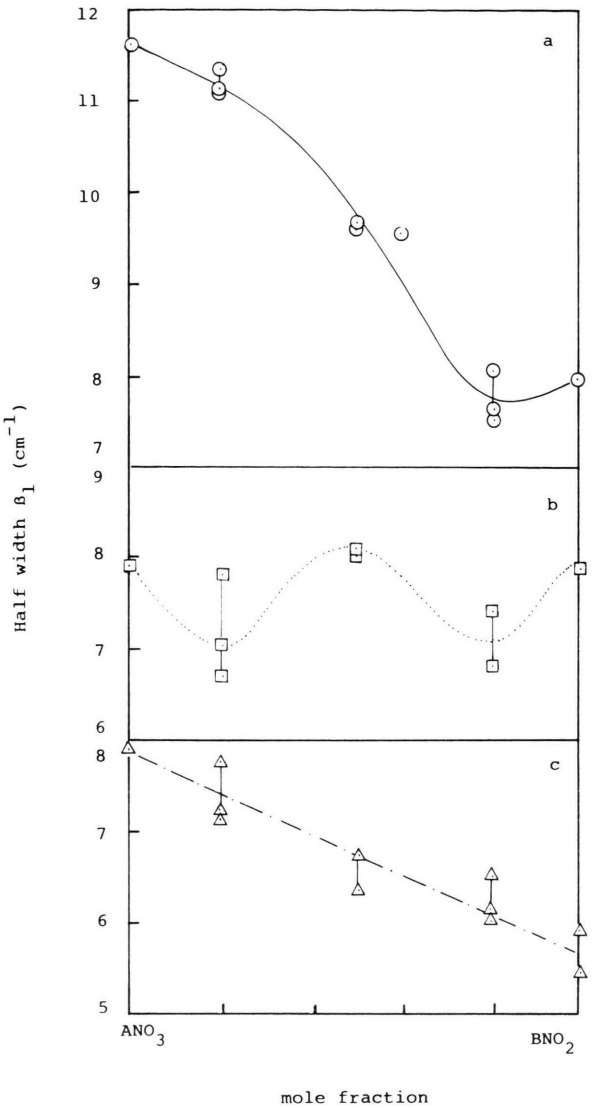

Fig. 3. Half width of A_1' mode of NO_3^- vs. mole fraction of molten ANO_3–BNO_2 systems.
a) A = Li, B = Na; b) A = Na, B = Na; c) A = Na, B = K.

Ubbelohde [22] explain this "red shift " as follows: the maximum absorption energy E_{max} is given by

$$E_{max} = E_1 + \frac{h^2}{8\, m r_0^2}, \tag{2}$$

where E_1 is the energy necessary for removing an electron from an anion, h is Planck's constant and r_0 is a distance obtained by subtracting the cation radius from the distance between a cation and an anion, given by Wyckoff et al. [28]. Differentiation of (2) with respect to temperature T results in

$$\frac{dE_{max}}{dT} = -\frac{h^2}{4 m r_0^3}\left(\frac{dr_0}{dT}\right). \tag{3}$$

Since r_0 spreads with increasing temperature, $dr_0/dT > 0$. Therefore $dE_{max}/dT < 0$, and the absorption spectrum shows "red shift" with temperature increase. Values of E_{max} obtained from our experiments were 236 nm (5.253 eV) at 260 °C, 240 nm (5.166 eV) at 360 °C and 242 nm (5.123 eV) at 415 °C. They gave a quite linear function with temperature. Here, the value of dE_{max}/dT amounts to $-6.8\,cm^{-1}K^{-1}$ for NO_3^- in molten $NaNO_3$–$NaNO_2$. Rhodes and Ubbelohde showed that $dE_{max}/dT = -5.6\,cm^{-1}K^{-1}$ for $LiNO_3$, $-3.4\,cm^{-1}K^{-1}$ for $NaNO_3$ and $-7.2\,cm^{-1}K^{-1}$ for KNO_3. Our value is twice larger than their value of $NaNO_3$. In Fig. 6a, E_{max} of NO_2^- also shows a slight "red shift" as temperature increases. This fact indicates that E_{max} is not only to be assigned to the intramolecular π-π^* transition in NO_2^- [29] but also to the influence of the empty orbital of Na^+. According to a calculation by the molecular orbital method [30], the highest occupied orbital of the NO_2^- anion is known to be -3.435 eV (-0.1263 Hartree). If the absorption

Table 2. Force constants of NO_3^- calculated by an approximate method using a Urey-Bradley potential for each molten composition ANO_3:BNO_2. K, H and F are the stretching force constants, the bending force constants and those between non-bonding atoms, respectively.

	K (mdyn/Å)	H (mdyn/Å)	F (mdyn/Å)
$LiNO_3$: $NaNO_2$			
10 : 0	5.802	0.570	1.600
8 : 2	5.810	0.551	1.587
4 : 6	5.704	0.548	1.596
2 : 8	5.732	0.532	1.609
$NaNO_3$: $NaNO_2$			
10 : 0	5.592	0.525	1.625
8 : 2	5.640	0.533	1.617
5 : 5	5.568	0.532	1.625
2 : 8	5.676	0.542	1.591
$NaNO_3$: KNO_2			
8 : 2	5.579	0.529	1.628
5 : 5	5.470	0.511	1.656
2 : 8	5.421	0.500	1.660
KNO_3	5.401	0.519	1.599

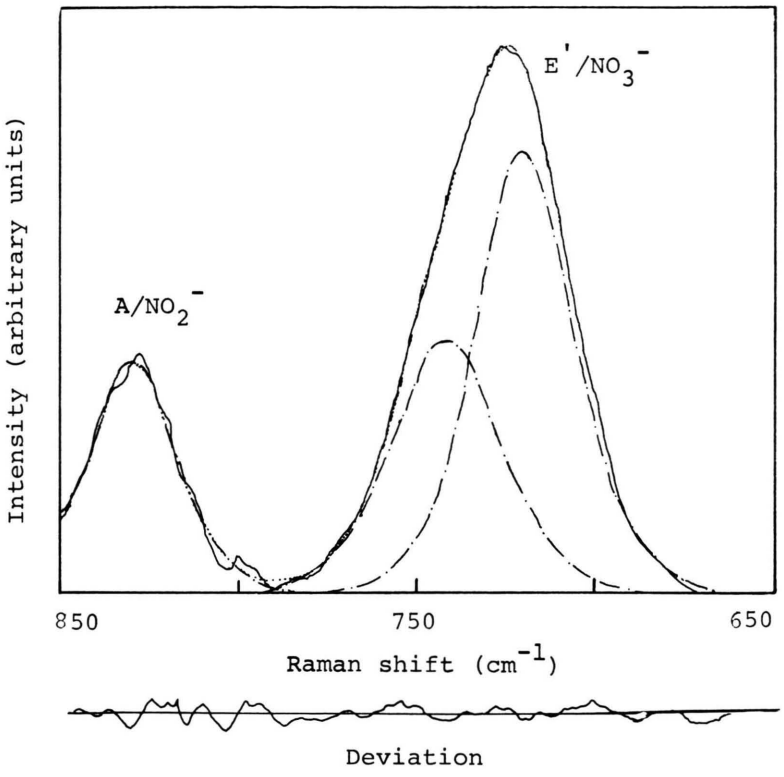

Fig. 4a) $LiNO_3 : NaNO_2 = 8 : 2$.

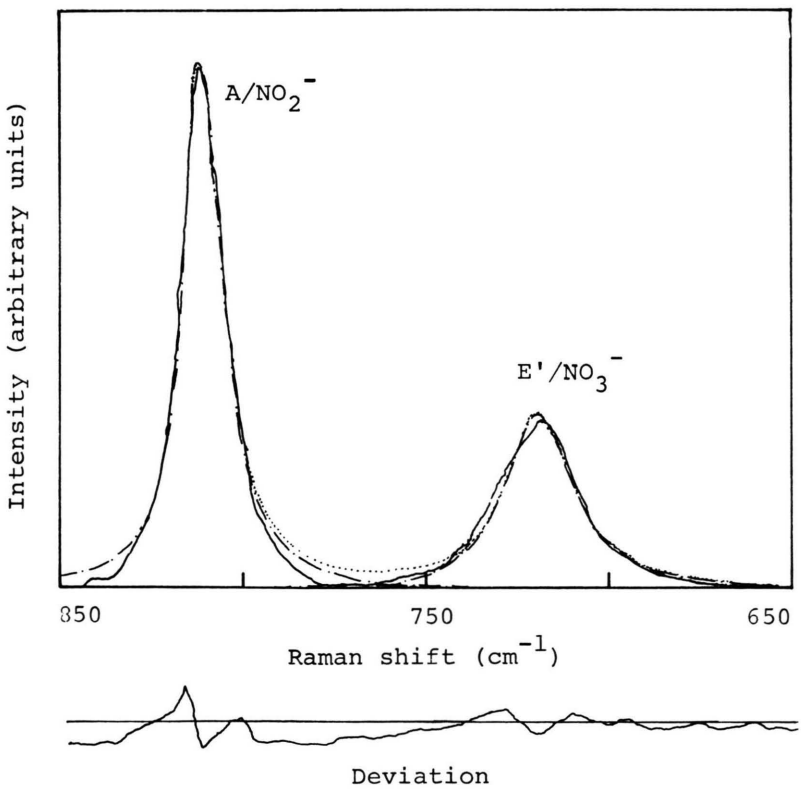

Fig. 4b) $NaNO_3 : NaNO_2 = 2 : 8$.

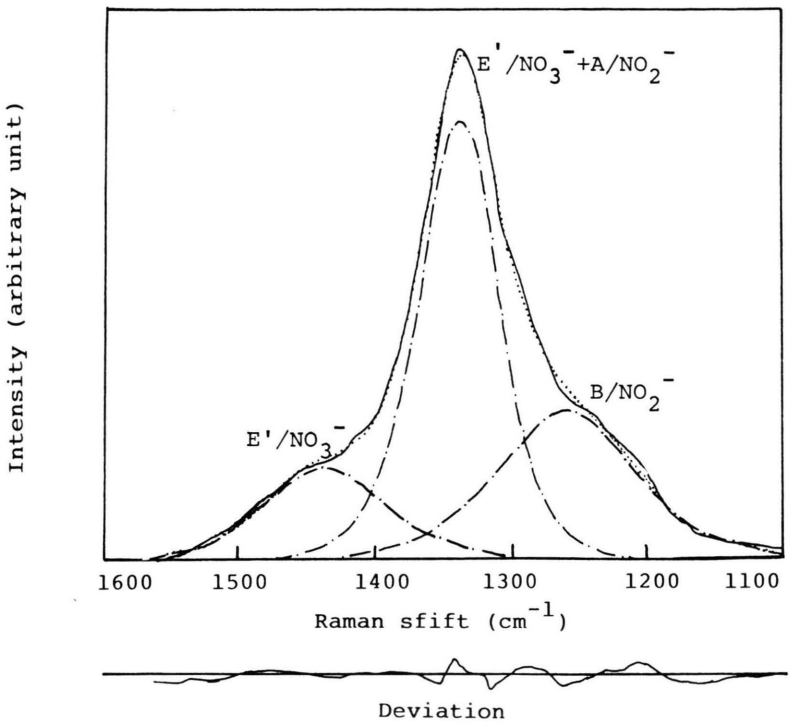

Fig. 4c) $LiNO_3$:$NaNO_2$ = 4:6.

Fig. 4. Three examples of the deconvolution of Raman bands into individual modes by use of a nonlinear least squares method. Deviation of the observed Raman profile from the calculated profile are indicated below.

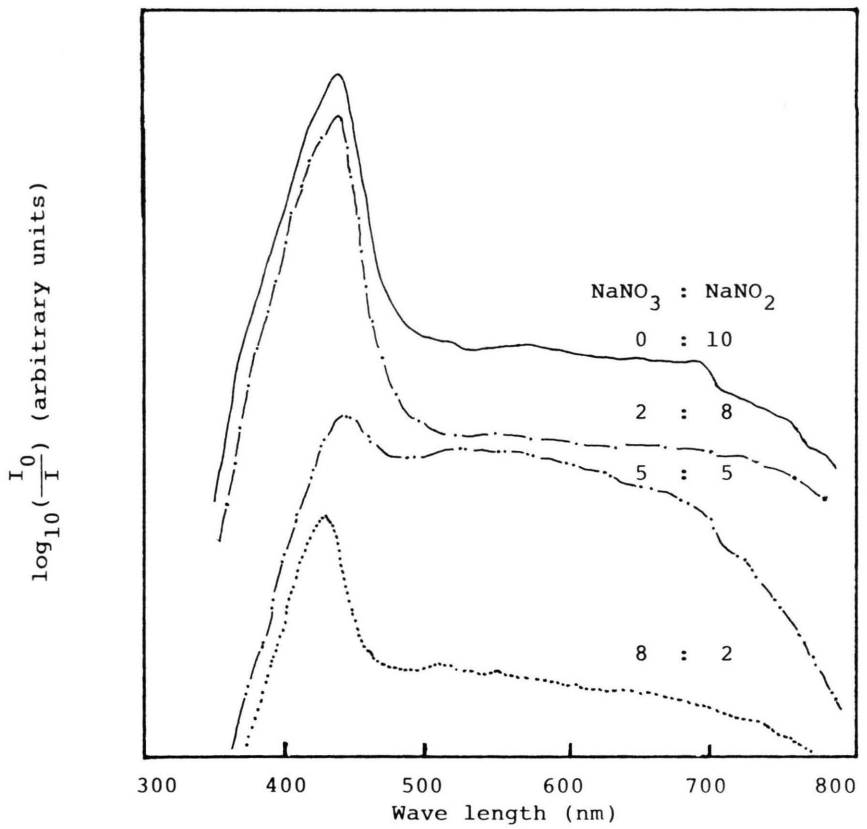

Fig. 5. Visible absorption spectra for various $NaNO_3$–$NaNO_2$ mixtures.

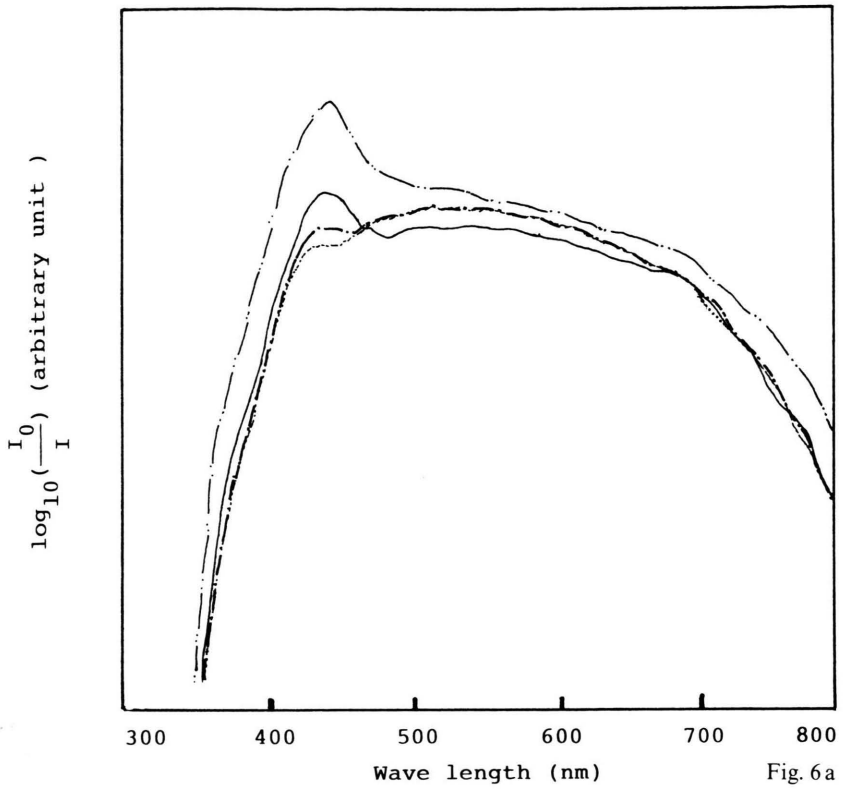

Fig. 6a

Fig. 6. Temperature dependence of visible absorption spectra (a) and ultraviolet absorption spectra (b) for the composition $NaNO_3 : NaNO_2 = 5 : 5$.
— ·· — 510 °C,
——— 410 °C,
— · — 360 °C,
····· 260 °C.

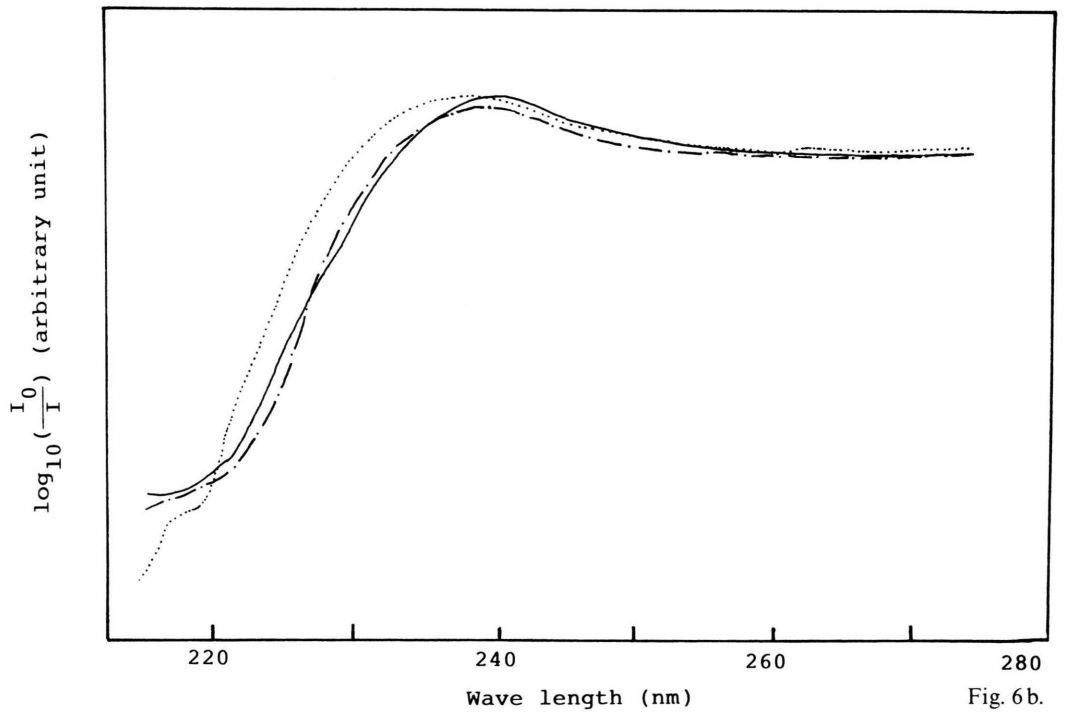

Fig. 6b.

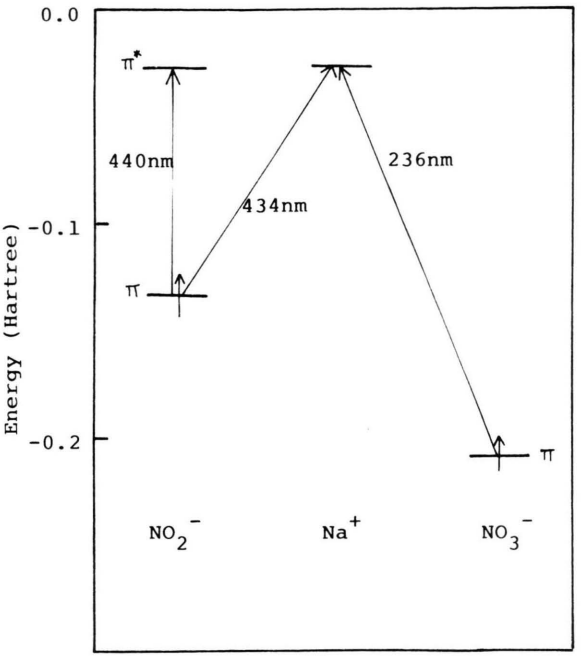

Fig. 7. Exprimentally estimated π^* level of NO_2^- and the empty orbital level of Na^+ in the molten $NaNO_3$–$NaNO_2$ system. the π levels of NO_3^- and NO_2^- are based on calculations with the molecular orbital method [30].

$E_{max} = 440$ nm is simply assigned to the π-π^* transition in NO_2^-, the energy level of the lowest unoccupied molecular orbital π^* becomes -0.617 eV (-0.022 Hartree). By use of the mentioned transition at 236 nm (260 °C) in NO_3^-, the energy level of the empty orbital of Na^+ can be determined to be -0.578 eV, which leads to an energy difference of 2.857 eV, (434 nm) between the empty orbital of Na^+ and the highest occupied molecular orbital (π) of NO_2^-. As shown in Fig. 7, this energy difference (434 nm) is very close to the mentioned π-π^* transition (440 nm), suggesting the existence of a strong interaction on approaching Na^+ to NO_2^- in the molten system. Such energetic assignments in Fig. 7 are verified, because Na^+ coexists with NO_3^- and NO_2^-.

Discussion

No Raman shifts in the A_1', $E'(\nu_3)$ and $E'(\nu_4)$ modes of NO_3^- and the A and B modes of NO_2^- show any drastic composition dependences in $NaNO_3$–$NaNO_2$ melts (Figures 2a–c). The visible absorptions of NO_2^- at 440 nm in Fig. 5 also undergo no appreciable shifts with composition. Therefore we conclude that the interaction between the anions, NO_3^- and NO_2^-, is much weaker than the ones between cations and anions. In other words, NO_3^- and NO_2^- exist independently, and Na^+ may exist between them. The A_1' mode of NO_3^- in Fig. 2a shifts by about 2 cm^{-1} towards higher wave numbers and its half width (Fig. 3) becomes narrower. These small anomalies in molten $NaNO_3$–$NaNO_2$ have not yet been rigorously accounted for in the present situation. In the molten $NaNO_3$–KNO_2 system, each Raman mode shifts almost linearly with composition, as shown in Figures 2a–c. We conclude therefore that NO_3^- and NO_2^- are statistically surrounded by Na^+ and K^+ ions according to the $NaNO_3$–KNO_2 melt composition. The molten $LiNO_3$–$NaNO_2$ system differs from the other systems. Each mode of NO_3^-, A_1' and $E'(\nu_3)$, and the A mode of NO_2^- show a strong composition dependence, especially for the A_1' mode of NO_3^-. To elucidate these results, we enumerate the characteristic differences among Li^+, Na^+ and K^+ as follows: Shannon's octahedral ionic radius [31] is 0.76 Å for Li^+, 1.02 Å for Na^+ and 1.38 Å for K^+. The volume occupied by a cation in the molten system is 0.439 $Å^3$ for Li^+, 1.06 $Å^3$ for Na^+ and 2.63 $Å^3$ for K^+. The polarizing power of Li^+ is 1.85, that of Na^+ 1.1 and that of K^+ 0.75 [32]. Judging from the differences enumerated above, the drastic composition dependence in Fig. 2a, where a little amount of $LiNO_3$ was mixed with $NaNO_2$, can be explained as follows: there remaines some free space after subtracting the values occupied by Na^+ and NO_2^- ions from the total volume of the molten $NaNO_2$ system. Li^+ would occupy this free space and attract several NO_3^- anions to form a "Li^+-nitrate associate" in molten $NaNO_2$, because Li^+ is smaller in size and stronger in polarizing power.

Smith and Boston [23] observed a "red shift" of the absorption maxima due to n-π^* transition in NO_3^- at ca. 300 nm as the size of the cation increases from Li^+ to Rb^+ in the UV spectra of pure alkali nitrate melts. They explained this "red shift" on the basis of the Franck-Condon and conservation-of-energy principles by showing that these n-π^* transitions are strongly related to the charge density of the N–O bond, and this shifts the electron density from the neighborhood of oxygen to that of nitrogen, and the strength of the N–O bond in-

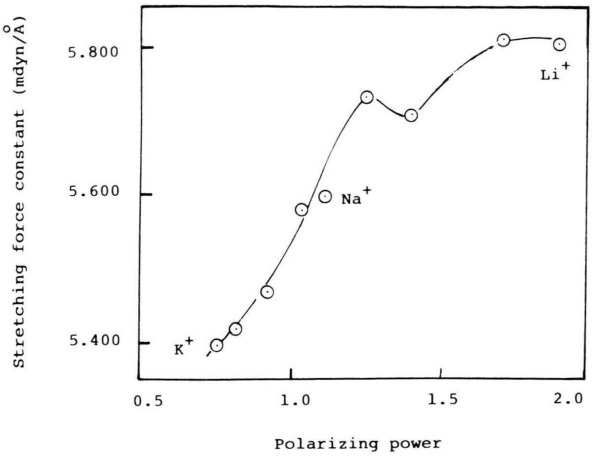

Fig. 8. Stretching force constant K (mdyn/Å) in Table 2 vs. averaged polarizing power for the molten ANO_3–BNO_2 systems. (A, B) = (Li, Na) and (Na, K).

creases as the size of the alkali cation decreases. Basing on this, the n-π^* transition in NO_3^- strengthens the N–O stretching force constant K, which is reflected in the Raman frequency $\tilde{\nu}$ (cm^{-1}) given by

$$\tilde{\nu} = \frac{1}{2\pi c}\sqrt{\frac{K}{M}}, \tag{4}$$

where M is the reduced mass and c is the speed of light. Thus, the Raman frequency shifts towards higher wave numbers as the size of the alkali cation decreases. In the "Li^+-nitrate associate", since NO_3^- is strongly perturbed by Li^+, the stretching force constant K in the N–O bond becomes stronger and the Raman frequencies shift to higher wave numbers for the molten composition $LiNO_3$:$NaNO_2$ = 2:8 in Figure 2a. We can say that the shift of the A_1' mode of NO_3^- originates in the formation of "Li^+-nitrate associate". With increasing Li^+ content towards the ratio $LiNO_3$:$NaNO_2$ = 5:5, every NO_3^- or NO_2^- is gradually shared by more than two Li^+, and there are fewer localized "Li^+-nitrate associates". Therefore the Raman shift of the A_1' mode of NO_3^- becomes smaller. As the concentration of Li^+ increases, the influence of Li^+ and Na^+ on NO_3^- is averaged and homogenized with composition. The absence of the drastic composition dependence in the Raman shifts in molten $NaNO_3$–KNO_2 is due to the larger volume and the smaller polarizing power of Na^+ as compared to Li^+. In Fig. 8 the stretching force constant K of NO_3^- is plotted against the averaged polarizing power of alkali cations in the molten system.

Anomalous changes with addition of small amounts of Li^+ to molten salts have also been observed in mobility measurements of Li^+ [33] or molecular dynamics simulations [34].

Acknowledgements

The authors wish to express their hearty thanks to Professor S. Maeda and Dr. S. Kobinata, Research Laboratory of Resources Utilization, Tokyo Institute of Technology, for their kind instructions and for permission to use their Laser Raman spectrophotometer. Thanks are also due to Professor I. Okada, Department of Electronic Chemistry, Tokyo Institute of Technology, for his useful discussions.

[1] O. J. Kleppa, J. Phys. Chem. **64,** 1937 (1960).
[2] O. J. Kleppa and L. S. Hersh, J. Chem. Phys. **34,** 351 (1961).
[3] O. J. Kleppa, J. Phys. Chem. **66,** 1668 (1962).
[4] O. J. Kleppa and S. V. Meschel, J. Phys. Chem. **67,** 2750 (1963).
[5] F. G. McCarty, L. S. Hersh, and O. J. Kleppa, J. Chem. Phys. **41,** 1522 (1964).
[6] G. J. Janz, U. Krebs, H. F. Siegenthaler, and R. P. T. Tomkins, J. Phys. Chem. Ref. Data **1,** 581 (1972).
[7] S. Takeuchi and K. Furukawa, Proc. Int. Symp. Phys. Chem. Process Metallurgy (Pittsburgh), Part 1, 133 (1969).
[8] H. Ohno and K. Furukawa, J. Chem. Soc. Faraday Trans. 1, **74,** 297 (1978).
[9] W. Bues, Z. Phys. Chem. **10,** 1 (1957).
[10] G. J. Janz and D. W. James, J. Chem. Phys. **35,** 739 (1961).
[11] J. K. Wilmshurst and S. Senderoff, J. Chem. Phys. **35,** 1078 (1961).
[12] J. K. Wilmshurst, J. Chem. Phys. **39,** 1779 (1963).
[13] S. C. Wait Jr. and A. T. Ward, J. Chem. Phys. **44,** 448 (1966).
[14] S. C. Wait Jr., A. T. Ward, and G. J. Janz, J. Chem. Phys. **45,** 133 (1966).
[15] J. H. R. Clarke, C. Solomons, and K. Balasubrahmanyam, Rev. Sci. Instrum. **38,** 655 (1967).
[16] R. E. Hester and K. Krishnan, J. Chem. Phys. **46,** 3405 (1967).
[17] D. W. James and W.-H. Leong, J. Chem. Phys. **51,** 640 (1969).
[18] M. Peleg, J. Phys. Chem. **77,** 2252 (1973).

[19] J. H. Clarke, Chem. Phys. Lett. **4,** 39 (1969).
[20] D. W. James and W.-H. Leong, Trans. Faraday Soc. **64,** 1948 (1970).
[21] M. H. Brooker, J. Electrochem. Soc. **126,** 2095 (1979).
[22] E. Rhodes and A. R. Ubbelohde, Proc. Roy. Soc. London **A 251,** 156 (1959).
[23] G. P. Smith and C. R. Boston, J. Chem. Phys. **34,** 1396 (1960).
[24] V. A. Maroni and E. J. Mathaway, J. Inorg. Nucl. Chem. **34,** 3049 (1972).
[25] P. I. Pretsenko and R. P. Shisholina, Russ. J. Inorg. Chem. **8,** 1436 (1963).
[26] Y. Iwadate, K. Kawamura, and J. Mochinaga, J. Phys. Chem. **85,** 1947 (1981).
[27] J. F. Kielkopf, J. Opt. Soc. Amer. **63,** 987 (1973).
[28] A. R. Ubbelohde, The Structure of Electrolyte Solutions, ed. W. J. Harmer, Chapman & Hall, London 1959.
[29] C. J. Ballhausen and H. B. Gray, Molecular Orbital Theory, p. 76, W. A. Benjamin Inc., New York 1965.
[30] J. F. Wyatt, I. H. Hiller, V. R. Saunders, J. A. Connor, and M. Barker, J. Chem. Phys. **54,** 5311 (1971).
[31] L. H. Ahrens, Nature London **174,** 644 (1954).
[32] R. D. Shannon, Acta Crystallogr. **A 32,** 751 (1976).
[33] C. Yang, R. Takagi, and I. Okada, Z. Naturforsch. **34 a,** 498 (1979).
[34] F. Lantelme and P. Turq, J. Chem. Phys. **77,** 3177 (1982).